HHS Public Access

Author manuscript

J Colloid Interface Sci. Author manuscript; available in PMC 2018 February 15.

Published in final edited form as:

J Colloid Interface Sci. 2017 February 15; 488: 258–268. doi:10.1016/j.jcis.2016.10.090.

Probing mucin interaction behavior of magnetic nanoparticles

Vijayakumar N. Boya[a,b], **Renn Lovett**[a], **Saini Setua**[a], **Vaibhav Gandhi**[a], **Prashanth K.B. Nagesh**[a], **Sheema Khan**[a], **Meena Jaggi**[a], **Murali M. Yallapu**[a,*], and **Subhash C. Chauhan**[a,*]

[a]Department of Pharmaceutical Sciences and Center for Cancer Research, University of Tennessee Health Science Center, Memphis, TN 38105, USA

[b]Department of Materials Science and Nanotechnology, Yogi Vemana University, Kadapa 516 001, AP, India

Abstract

In this study, we developed iron oxide based magnetic nanoparticles (MNPs) by precipitation of iron salts in the presence of ammonia and created four different formulations: without functionality (plain MNPs, no coating), with β-cyclodextrin (MNPs+β-CD) or pluronic 127 polymer (MNPs+F-127), and both β-cyclodextrin and pluronic 127 polymer (MNPs+β-CD-F-127) functionality for its efficient use in mucosal delivery. We studied the interaction and/or binding behavior of these MNPs formulations with porcine stomach mucin using steady-state fluorescence spectroscopy, and then quantified the bound mucin from absorption studies. Toxicity of these MNPs against cervical cancer cells and red blood cells was evaluated. *Ex-vivo* studies were performed using freshly collected gastrointestinal, ovarian, pancreas and colon organ tissues of pig to evaluate binding and uptake phenomenon of MNPs. Transport studies of these MNPs in mucin was evaluated using Boyden's chamber assay. All these studies together suggest that the MNPs+β-CD-F-127 formulation was strongly interacted with mucin and interestingly transported through mucin compared to other MNPs formulations. Hence, MNPs+β-CD-F-127 formulation could be a good candidate for the mucoadhesive biopharmaceuticals and drug delivery system.

Graphical abstract

*Corresponding authors at: Department of Pharmaceutical Sciences and the Center for Cancer Research, University of Tennessee Health Science Center, 881 Madison Ave, Memphis, TN 38163, USA (M.M. Yallapu). Department of Pharmaceutical Sciences and the Center for Cancer Research, University of Tennessee Health Science Center, 226 Cancer Research Building, 19 South Manassas, Memphis, TN 38163, USA (S.C. Chauhan). myallapu@uthsc.edu (M.M. Yallapu), schauhan1@uthsc.edu (S.C. Chauhan).

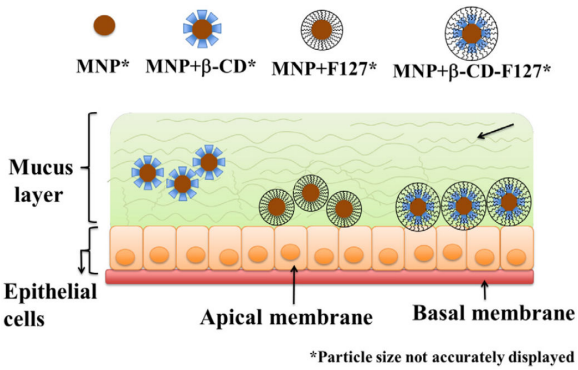

Keywords

Magnetic nanoparticles; Drug delivery; Mucoadhesive pharmaceuticals; Mucin; Cancer

1. Introduction

Mucus is a viscoelastic and biopolymeric gel composed of cross-linked and entangled mucin fibers, present on mucosal surfaces of the eyes, respiratory, gastrointestinal, and female reproductive systems. Mucus is primarily composed of glycoprotein, proteoglycans, and lipids [1–4]. Mucins are the major parts of the heavily glycosylated proteins present in the mucus gel with polypeptide backbones [5–7]. Under normal physiological conditions, mucus composition, viscoelasticity, mucin-to-water ratio, protein, lipid, and ion contents are tightly maintained [8]. This stimulates a protective mechanism of the body that has an excellent ability to immobilize and remove foreign materials such as pathogens, bacteria, and even drugs, by different mucus clearance mechanisms [9–14]. However, unregulated expression of mucin from the mucosal structures causes imbalance and leads to dysfunction and demise of biological systems [14–18]. This may lead to cystic fibrosis, chronic obstructive pulmonary disease, asthma, inflammatory bowel disease, ulcerative colitis, Crohn's disease, etc. [14,19–22]. Overexpression of various mucin(s) is also linked to pancreatic, ovarian, breast, lung, and colon cancer initiation, progression, and metastasis [23–32]. The other major difficulty associated with mucin is the trapping of colloidal drug delivery systems, which limits the bioavailability of the drug at a desired target site in treating malignancy [33–36]. Cervical cancer is further characterized by presence of abundant epithelial mucus on the surface of the cervix. Because of this, most of the chemotherapies often fail due to limited concentration of drug reaching the mucosal tissue, and/or blocking of drug penetration through the mucous layer(s).

Drug delivery technologies, especially nanoparticle-based drug delivery systems, have proven beneficial for human use and are being extensively studied in clinical trials. These nanocarriers exhibit a number of anticipated characteristics such as protection of loaded therapeutics, sustained and local controlled release of therapeutics, enhanced cellular and sub-cellular uptake, and deep tissue penetration. However, conventional drug delivery systems are likely trapped by a mucus layer *via* steric or adhesive forces, which leads to clearance of particles by mucus. These particles fail to cross the outermost layers of the

mucus barrier (1 μm to few hundred microns) to impose therapeutic actions. Therefore, it is a challenge to design a new drug delivery system that possesses mucoadhesive property along with mucus penetration capacity. Together, they can prolong their residual time or target specific regions for translocation through the mucus layers. The advent of mucoadhesive drug delivery systems opened up new avenues and demonstrated an increase to the dosage form's residence time at the site of administration with improved penetration through the mucous of epithelium. Both mucoadhesive and mucus penetrating drug delivery systems have demonstrated that the surface properties of the incorporated polymer excipients, in preparation of nanoparticles, are playing an important role in improving the adhesion and translocation of the particulate systems with mucus layers [2,34–40]. For example, PEGylated poly(methyl vinyl ether-co-maleic anhydride) nanoparticles with PEG-2000 form a brush layer to decrease interaction with mucus but increase its contact with the intestinal mucosa [40]. Poly(vinyl alcohol), chitosan (CS), and poloxomer (PF68) coatings on the biodegradable PLGA nanoparticles provide neutral, positive, and negative surface charges, which play an important role in carrying the nanoparticles to the bronchial airway barrier and epithelial cells [21]. Ensign et al. [41] demonstrated that pretreatment of cervicovaginal mucus (CVM) liquids with pluronic F-127 can enhance the transport of native polystyrene (PS) beads compared to polyethylene glycol (PEG)-PS beads. In another recent study, self-assembled nanoparticles based on cell penetrating peptides can overcome the mucus diffusion barrier and the epithelium absorption barriers [34] for oral delivery of insulin. Surface PEG density on PLGA has a significant impact in transport in mucus. It has been demonstrated that an increase in PEG density increases the transport of PLGA nanoparticles through CVM [36]. All these studies suggest that functionalized nanoparticles have a good possibility to interact/transport/diffuse effectively with the mucus layer of different mucosal structures. Altogether, PEGylated nano- and micro-particle have shown superior mucoadhesion and facilitated mucosal transport for improved drug delivery. Considering this fact, we have engineered a unique, magnetic nanoparticle formulation, which has shown improved therapeutic benefit of loaded therapeutic molecules [42]. This formulation not only contains PEG groups in pluronic polymers but also β-cyclodextrin. In order to develop this nanosystem for mucosal delivery, we aimed to study its mucoadhesive and mucus transportation phenomenon. Therefore, we aimed to study the effect of β-cyclodextrin and/or pluronic 127 coating on magnetic nanoparticles at mucin interface, i.e., MNPs-Mucin bio-interface. We have chosen these polymers as a coating material because of their extensive use in the pharmaceutical industry as excipients. We have used mucin derived from porcine stomach for all *in vitro* studies, as it closely resembles human mucin. For *ex-vivo* studies, freshly collected porcine tissues of GI, pancreas, ovarian and colon were used. Transport of MNPs in mucin layer solution was studied using the Boyden's chamber. Our present study suggests that MNPs+β-CD-F-127 formulation strongly interacts with mucin and can effectively transport through the mucin layer. Thus, it could be a good candidate for mucoadhesive biopharmaceuticals.

2. Materials and methods

2.1. Materials

All of the chemicals and regents used in this work were purchased from Sigma Chemical Company (St. Louis, MO) and used as such unless otherwise stated. MilliQ water or 1X PBS was used throughout our study.

2.2. Preparations of magnetic nanoparticles

Iron oxide magnetic nanoparticles (MNPs) are prepared by following the procedure developed by Yallapu et al. [42]. In brief, 300 mg of iron (II) chloride tetrahydrate (⩾99%) and 800 mg of iron (III) chloride hexahydrate (98%) were reduced with ammonium hydroxide solution (28% NH_3 in water, purified by distilled water) under stirring in presence of dispersant/polymer. Once the salts were dissolved, nitrogen gas was purged for about 10 min, and then ammonia was added by the drop under vigorous stirring. The mixture was kept under stirring overnight, and then washed several times with water using strong magnets. Finally, the particles were suspended in water to obtain 10 mg/ml concentration. A total of four different formulations were made using β-cyclodextrin (BioReagent grade, ⩾97%) (MNPs+β-CD), pluronic 127 (BioReagent, contains 100 ppm BHT) (MNPs+F-127), twin coated with both these polymers (MNPs+β-CD-F-127), and with uncoated magnetic nanoparticles (uncoated MNPs). In case of twin-coated samples, similar protocol was used as stated, with the exception of adding the pluronic 127-polymer solution after the reduction of iron salts and into iron oxide nanoparticles.

2.3. Size and zeta potential measurements

The size and zeta potential of the MNPs were measured using the dynamic light scattering technique by Zetasizer (Nanoseries, Malvern, UK). 10 μl of 10 mg/ml particles were dispersed in 1 ml of water and probe sonicated (VirSonic Ultrasonic Cell Disrupter 100, Vir Tis) for 30 s. This solution was used to measure the size of the particles. The effective mean diameter of the nanoparticles was obtained from three runs of each sample measured for 3 min. The data presented was the average of a minimum of three independent experiments.

Zeta potential is an indicator of the charge that is present on the surface of nanoparticles, which deals with stability of formulations and interaction with cellular membranes. The same instrument was used to measure the zeta potential of diluted MNPs using the principle of electrophoretic mobility under an electric field. The data presented was the average of a minimum of three independent measurements for 9 min each. In the similar manner, size and potential of the mucin bound MNPs were measured by dispersing 10 μl of 10 mg/ml particles in 1 mg/ml mucin solution in water.

2.4. Mucin binding characterization

Physical characterization of mucin bound MNPs was confirmed by Fourier transforming infrared spectroscopy (FTIR), X-ray diffraction (X-RD), and thermogravimetric analysis (TGA). FT-IR spectral data (between 4000 and 750 cm^{-1}) of samples was acquired on the Universal ATR Sampling Accessory plate using a Spectrum 100 FTIR spectrophotometer (Waltham, MA). The X-ray diffractograms were collected over the 2θ range of 25°–70°

using a Rigaku D/Max-B diffractometer (Rigaku Americas Corp, Woodlands, TX) with cobalt-alpha radiation (λ = 1.5 Å). The measurements were recorded by an operating system at 40 kV and 40 mA. TGA was performed using a Q50 thermogravimetric analyzer (TA Instruments, New Castle, DE) with a heating rate of 10 °C/min under a dry nitrogen atmosphere (a flow rate of 10 mL/min) from 50 °C to 500 °C.

2.5. Study-state fluorescence spectroscopy

Steady state fluorescence spectroscopy was used to study the instantaneous adsorption or binding of mucin on MNPs on a SpectraMax Plus plate reader (Molecular Devices, Sunnyvale, CA). Intrinsic fluorescence of 0.5 and 1 mg/ml mucin solution in 1X PBS was measured by titrating with 0–100 μg/ml MNPs. Fluorescence decay profiles were obtained by exciting mucin solution at 280 nm and at the emission set from 300 to 500 nm. The binding constant and number of binding sites (n) were calculated from the following equation:

$$\frac{F_0 - F}{F_0 - FS} = \left\lfloor \frac{MNPs}{Kdiss} \right\rfloor n$$

where F_0, F and F_S are the fluorescence area under the curve of emission of mucin, and mucin titrated with various MNPs, respectively. A representative spectrum was presented in figures for each formulation but the final values in table were reported as an average of three independent measurements.

2.6. MNPs-mucin absorption studies

The extent of interactions between mucin and MNPs was measured by incubating the 0.1–1 mg/ml concentration of particles with 1 mg/ml of mucin solution in water. MNPs were mixed with a mucin solution and sonicated for 10 s. The solution was then incubated for different intervals of time in 1.5 ml Eppendorf tubes kept on a shaker (Reciprocal 30, Labnet) at room temperature. At pre-determined time points, tubes were centrifuged (Eppendorf centrifuge 54 5 D) at 13,000 rpm for 1 min to separate unbound mucin and mucin-bound MNPs. Absorbance of the supernatant solutions (un-bound mucin) was measured at 280 nm (SpectraMax Plus M2e plate reader, Molecular Devices, Sunnyvale, CA). From these values, the concentration of bound mucin on MNPs was calculated. In a similar manner, the interactions of mucin with MNPs were studied at a fixed MNPs concentration of 250 μg/ml with varied mucin concentration from 0.1 to 1 mg/ml. All of these measurements were carried out in three independent experiments.

2.7. Cell proliferation studies

Human cervical carcinoma (SiHa) cell line (American Type Cell Culture, Manassas, VA) was maintained in Dulbecco's Modified Eagle Medium (DMEM) (HyClone Laboratories, Inc., Logan, UT) by supplementing with 10% fetal bovine serum (Atlanta Biologicals, Lawrenceville, GA) and 1% penicillin/streptomycin (Gibco BRL, Grand Island, NY). This cell line was used to study the toxicity profile of MNPs and mucin-bound MNPs. 5000 cells/well were seeded in 96-well plate and kept in a cell culture incubator (InC Safe CO_2

incubator, Sanyo Scientifics) for 24 h. The cells were then treated with 10, 50, and 100 μg/ml concentrations of MNPs of varying formulations. The same concentration of PBS was also used (control). After 48 h, the cells were washed with 1X PBS and incubated with MTS reagent for 2 h. The absorbance was measured at 490 nm, using a microplate reader (Cytation 3 imaging reader, BioTeK). The percentage of viable cells was calculated by comparing absorbance of treated cells with PBS. All the measurements were carried out five times.

2.8. Toxicity and hemolysis assay

Freshly collected sodium citrate anticoagulant human whole blood of a healthy donor was used to examine the hemolysis potential, and to obtain a quantitative measure of the hemoglobin release from red blood cells (RBCs) of MNPs and mucin bound MNPs. The RBC suspension (200 μl) was incubated with 5, 10, and 20 μg/well of MNPs and mucin bound MNPs (2.5 mg/ml) in Eppendorf tubes in an incubator for 60 min at 37 °C. Sodium dodecyl sulfate (SDS, 1 mg/ml) was used as a positive (100% lysis) control while 1X PBS was used as a negative (0%) control in this experiment. The sample tubes were centrifuged at 2000 rpm for 5 min. The supernatant (100 μl) was transferred to a 96-well plate to measure the concentration of hemoglobin released at 510 nm absorbance by using a plate reader (Cytation 3 imaging reader, BioTeK). From the supernatant solutions, a few drops are smeared on a glass plate and images of the RBC cells were taken using an Olympus camera. The percentage of hemolysis was calculated using the following equation:

$$\%Hemolysis = \frac{(Absorbance\ of\ sample - Absorbance\ of\ negative\ control)}{Absorbance\ of\ positve\ control} \times 100$$

2.9. Ex-vivo studies of dye tagged MNPs on different pig tissues

Fresh tissues from different organs of a pig were collected from a butcher house immediately after scarifying the pig. The tissues were washed with water, 1X PBS, and with DMEM. The GI tissue was cut into small square pieces of 250–350 mg and washed with 1X PBS without disturbing the mucus layer. In order to quantify the uptake and/or transport of MNPs by tissue, nanoparticles were tagged with coumarin-6 dye by incubating the 250 μl of 2.5 mg/ml dye in acetone with 1 ml of 10 mg/ml particles under stirring overnight. For all of these experiments, DMEM media without serum was used.

In order to understand the uptake and/or transport of MNPs with time, a 500 μg/ml MNPs particle dispersions were made in DMEM media. GI tissue was incubated at room temperature for 30, 60, 180, and 360 min in these MNP dispersions in such a way that the mucus layer of the tissue was facing upward in a 12-well tissue culture plate. At each time point, the tissue was taken out from the incubating media and washed with 1X PBS to remove peripheral adhered nanoparticles. The tissue was then incubated overnight in 1 ml of acetone in order to extract the dye present in the MNPs, which is an indication of uptake by the tissue. From this, 100 μl of acetone was taken in a 96-well plate and absorbance of the dye was measured at 490 nm (Cytation 3 Imaging reader, BioTeK). Finally, the amount of MNPs uptakes by the tissues were calculated from the dye standard curve, derived from

different concentrations of dye in acetone. All of the measurements were carried out in three independent experiments. The same protocol was followed in order to evaluate the amount of uptake of dye MNPs in the tissues (150–250 mg) of pancreas, ovarian, and colon organs of a pig. Again, all of the measurements were carried out in three independent experiments.

Prussian blue staining was used to evaluate the biding and transportation of MNPs in GI tissue. For this, GI tissue, with the mucus layer facing upward, was placed in 12-well plate. Varying concentrations of dye tagged MNPs dispersed in DMEM media was added and incubated for 3 h. After the incubation period, the tissue was removed and washed with 1X PBS, then cross-sectioned and stained with 1 ml of 10% ferrous ammonium cyanate in 1N HCl for 1 h. This process turns the iron a blue color. The images of the stained tissues were taken with a regular photographic camera.

2.10. Boyden's Chamber assay

Boyden chamber assay was used to evaluate the transport/penetration of MNPs through mucin. We used 12-well cell culture plates with 8 μm pore size membrane inserts. The micro porous membrane was separated into the upper and lower compartments and was hydrated by immersing for 30 min in 1X PBS before use. Porcine stomach mucin powder solutions with 0.5 and 1 mg/ml concentration were prepared in 1X PBS and placed in the upper chamber. The same quantity of 1X PBS was place in the lower chamber. Coumarin-6 dye tagged MNPs were added to the mucin solutions in the upper chamber to get a final MNPs concentration of 500 μg/ml. The plates were kept at room temperature in dark conditions. A 200 μl sample of solution from the lower chamber was collected at regular intervals of time (30, 60, 180, 360 min, and 24 h) in 1.5 ml Eppendorf tubes. The collected samples were centrifuged at 13,000 rpm for 10 min. The supernatant liquid was discarded and 1 ml of acetone was added to the MNPs pellet to extract the dye present in the MNPs. Finally, absorbance of dye solutions was measured for all of the samples at 490 nm (Cytation 3 Imaging reader, BioTeK), taking 100 μl in a 96-well culture plate. The amount of dye present in the MNPs was calculated using dye standard curve in acetone. All of the measurements were carried out in three independent experiments.

2.11. Data analysis

Particle size, zeta potential, fluorescence, absorption, hemolysis, tissue uptake and Boyden's chamber experiments were carried out in triplicate, whereas, cell proliferation was conducted five times. All experimental results were calculated using Microsoft Excel 2013 software and expressed as mean ± standard error of the mean (S.E.M.). All graphs were plotted using Graph pad Prism 5 software.

3. Results and discussion

Development of a successful mucoadhesive drug delivery system with mucus penetrating capacity is currently sought to improve therapeutic delivery at mucosa. These particles are designed to adhere to mucosal membrane through various physical interaction and thus can be enabled to prolong therapeutic molecule retention. Based on the properties of mucoadhesive nanoformulations and its interaction with various mucosal layers,

nanocarriers can be developed for oral, nasal, ocular, vaginal, buccal, and airway drug delivery. Hence, we studied the interaction and subsequent transport of developed MNPs with a model mucin (porcine stomach). MNPs were prepared by reducing the iron salts and subsequent coatings with muco-adhesive/penetrating polymers following the procedure outlined in the schematic representation displayed in Fig. 1. Although there are numerous theories and mechanisms of mucoadhesion such as wetting, electronic, adsorption, diffusion, fracture and mechanical based mechanisms, we focused on adsorption and diffusion studies with mucin. These two mechanisms were evaluated by measuring the following: the size of nanoparticles, instantaneous fluorescence quenching, mucin binding on nanoparticles, binding and penetration of nanoparticles in *ex-vivo* tissues, and transport of nanoparticles in Boyden's chamber.

3.1. Particle size and zeta potential

Size and zeta potential of the nanoparticles can govern binding and transporting capabilities in mucus. Mucus is a viscous gel composed of cross-linked mucin fibers. Particles are small enough to bind to these mucin fibers and slick enough to slide through cross-linked networks (often 500 nm) to deliver payload efficiently at mucosal tissue, rather than exhibiting quick particle elimination. Particles with greater diameters will have less surface area, which can affect the binding. These particles also present limited ability to transport freely because they may only move through larger diameter channels [38,43–47]. Hence, it is important that particles should have an optimum size range. The results of size and zeta potential of the MNPs and MNPs-mucin are presented in Fig. 2Aand B. The average particle size of the native MNPs, MNPs+β-CD, MNPs+F-127, and MNPs+β-CD-F-127 are about 110, 122, 129, and 117 nm. Their size increased to 195, 209, 232 and 207 nm, respectively, after incubation with mucin. This suggests that the mucin was able to bind or immobilize on the surfaces of MNPs instantaneously. The increase in overall size of particles attributed to the hydrodynamic and globular state of mucin bound on nanoparticles. Additionally, increase in particle size upon mucin binding leading to extent of mucin protein interaction between particles, not just by the coating of mucin on individual particles. Moreover, the zeta potential of the MNPs has also varied due to their interactions with mucin. This is acceptable because additional coating by mucin protein which is negative zeta potential in nature further decrease overall zeta potential behavior. The potential values varied from −3 to −8 mV in the case of native MNPs and −6 to −13 mV in case of MNPs-mucin. These negative potential values suggest that the particles can bind with mucin and can expect better transport behavior in mucin.

3.2. Characterization

The presence of mucin on the surface of nanoparticles was confirmed by Fourier transform infrared spectroscopy (FTIR), X-ray diffraction (X-RD), and thermogravimetric analysis (TGA). The FTIR spectra of nanoparticles MNPs, MNPs+β-CD, MNPs+F-127, and MNPs +β-CD-F-127 exhibits various characteristic peaks similar to our previous report (Fig. 3A). A distinct spectral shift from 3370 to 3220 cm^{-1}, an appearance of specific peaks at 2920, 2850, 1540 cm^{-1}, and a change of peak intensities at 1635, 1230, and 1050 cm^{-1} corroborates to protein (mucin on nanoparticles) presence on the surface of nanoparticles (Fig. 3B). The XRD pattern of MNPs, MNPs+β-CD, MNPs+F-127, and MNPs+β-CD-

F-127 shows six well-resolved diffraction peaks at 30.1, 35.5, 43.1, 53.5, 57.2, and 62.8° (indexed to the 220, 311, 400, 422, 511, and 440 planes), which confirms the face centered cubic spinel phase of nanoparticles (Fig. 3C). MNPs-mucin nanoparticles exhibit two additional diffraction peaks at 31.3° and 45.2° indicating mucin presence on the surface of nanoparticles (Fig. 3C). Parent MNPs, MNPs+β-CD, MNPs+F-127, and MNPs+β-CD-F-127 does not show considerable weight loss, whereas mucin bound nanoparticles undergo rapid degradation due to mucin existence on the surface of nanoparticles (Fig. 3D).

3.3. Florescence quenching and binding rate

The adsorption or binding of mucin on a nanoparticles system takes place upon intimate contact between surfaces of nanoparticles and mucin chains *via* multiple adhesive forces, including, hydrogen bonding, electrostatic attraction, hydrophobic interaction, and physical entanglement [48–50]. The extent of mucin binding on nanoparticles can alter the structural confirmations of mucin macromolecules. This can be another factor in nanoparticles-nanoparticles interactions, which finally results in creating nanoparticles-mucin network systems. To improve or alter the binding of mucin, it is important to modify the surface characteristics of nanoparticles such as functional groups, surface charge, and also the diameter of the nanoparticles [36,51,52] by coating with relevant substances. It has been demonstrated that hydrophilic polymers, especially electrically charged polymers, show good mucoadhesive capacity compared to non-charge hydrophilic polymers [53,54]. In the present case, the surface properties of MNPs were modified by coating with β-CD or F-127, or a combination of β-CD and F-127.

Adsorption of mucin and the rate at which it adsorbs onto nanoparticles is very useful in designing mucosal delivery particulate systems. This phenomenon can be assessed by using a fluorescence quenching technique [36,42,44,55]. This is a widely used technique to study the binding and conformational changes upon association with small molecules, membranes, and nanoparticles [42,55–58]. This technique measures fluorescence quenching of biomacromolecule(s) due to the variety of molecular interactions, including ground-state complex formation, collisional quenching, excited state reactions, molecular rearrangements, and energy transfer. These different mechanisms are classified as either static-quenching (ground-sate complex) or dynamic-quenching (collisional quenching) [59]. The steady-state fluorescence quenching plots are displayed in Fig. 4A–D in 1 mg/ml mucin for all four unique MNP formulations. In all of the MNP formulations, we observed that florescence quenching of mucin increased gradually with an increase in the concentrations of MNPs from 0 to 10 μg/ml. This may be due to part of the tryptophan residue of mucin that is involved in the adsorption process on MNPs. We have not observed any bathochromic shift at λ_{max} = 340 of mucin, which suggests that the tryptophan residue is buried [60,61]. Further, the number of adsorption sites on MNPs and the adsorption constants were calculated using the florescence quenching data. The values are presented in Table 1 [42]. Even though the florescence quenching of mucin is increased with addition of MNPs, the MNPs+β-CD-F-127 formulation has showed a slightly higher rate of quenching than others. This directly reveals the role of surface properties of MNPs in binding mucin. F-127 is a tri-block copolymer with hydrophilichydrophobic-hydrophilic regions spaced with poly(ethylene glycol) structures and separated by hydrophobic chains, whereas

bcyclodextrin is a cyclic oligosaccharide with hydrophobic core and hydrophilic heads. This allows for more potential site interaction on the overall surface of MNP, which creates increased binding with mucin compared to only β-CD (MNPs+β-CD) and F-127 (MNPs +F-127) coated surfaces. Both of these have showed considerable comparable binding of mucin. This was further indicated from the number of adsorption/binding sites calculated (Table 1). It has been demonstrated that the PEG coated nanoparticles surface reduces the binding with mucin and increases the transport, but it depends on the molecular weight and surface thickness of the PEG [36,40,47,62,63]. In the present study, even though the surface of MNPs+β-CD-F-127 has PEG structures, it showed good binding. This may be attributed to the fact that the PEG structures on MNPs are originated from tri block copolymer of F-127 and not the pure PEG chains. From this study, it is imminent that the surface of MNPs has a significant role on the interactions and binding with mucin. Hence, we decided not to proceed with plain MNPs (uncoated) and the MNPs+F-127 formulation, which has similar biding characteristics of MNPs+β-CD, in our later experiments.

3.4. MNPs and mucin interactions

There are various methods to estimate the amount of protein bound on to the particles [36,42,53,54]. We used a simple absorption method to estimate the amount of mucin binding on MNPs by changing concentrations of mucin and MNPs at different time points. These studies delineate the adsorption of mucin on to the surfaces of nanoparticles, which governs the extent of mucin and nanoparticles associations, including self-assembly into extended particle clusters, which can be used to evaluate mucoadhesive behavior of nanoparticles [64]. The amount of mucin bound on the MNPs, with time, by changing the concentration of mucin from 100 to 1000 μg/ml at fixed 250 μg/ml concentration of MNPs, are displayed in Fig. 5A. As the concentration of mucin increases, the amount of bound mucin also increased. For all the concentrations of mucin, most of the mucin was bound onto the MNPs within first hour of incubation and increased moderately with increase in time of incubation, but did not follow any trend. In the case of MNPs+β-CD-F-127, the amount of mucin bound is little more compared to their MNPs, but decreases slowly as the time increases up to 24 h. This may be due to the complex nature of the surface of MNP, or because of the dual coating given with both β-CD and F-127 polymers as discussed above. This is quite interesting and could be useful in designing novel particulate systems for mucosal delivery applications. It not only shows mucus adhesion, but also shows that it can become unbound with time, which can help with distributing and transporting within the mucin.

The results of bound mucin with varied concentration of MNPs (from 10 to 500 μg/ml at 1000 μg/ml of fixed mucin concentration for all MNP formulations) are presented in Fig. 5B. This study was limited to one and 3-h time points because the incubation time has not shown a significant change in the amount of bound mucin. The MNPs+β-CD-F-127 formulation showed a higher amount of mucin binding than other MNPs. As the concentration of MNPs increased, the amount of bound mucin also increased. The concentration of nanoparticles is significant in terms of the maintenance of the mucin layer. A higher amount of particles can disrupt and collapse the mucin structure, leading to the rearrangement of the mucin network [63,65]. This can result in the loss of barrier properties of mucin and increase the diffusion rates of particles.

3.5. Cell culture and red blood cells

Cell proliferation studies using different concentrations of MNPs were performed on SiHa cervical cancer cells and the results are presented in Fig. 6A. All the MNPs have shown the cell viability to be about 95%, with no increase or decrease trends, even with increase in concentration of MNPs. This suggests that the MNPs are not toxic to SiHa cells.

When any nanoparticle system interacts with blood cells, if toxic, unwanted side reactions will occur as soon as it is administered into the human body. Hence, we have studied the toxicity of the developed MNPs along with mucin-bound MNPs using PBS as the negative control and sodium dodecyl sulphate (SDS) as the positive control. The results, found by performing hemolysis experiments, are presented in Fig. 6B. All MNPs have shown very little (<2%) hemolysis, which is almost negligible. Even mucin bound MNPs showed very low levels (<4%) of hemolysis. This data suggest that these formulations are non-toxic and hemocompatible, and thus, can be useful for pre-clinical/clinical applications.

3.6. Ex-vivo studies on pig tissues

In order to verify the mucoadhesive and muco-penetrating characteristics of MNP formulations, we have performed *ex-vivo* studies of pig tissues consisting of GI, pancreas, ovarian, and colon tissues, by varying the concentration of MNPs and time. These studies describe the binding extent of the interaction of MNPs with the mucin layer, and facilitate the uptake process by this tissue. For quantitative estimation of uptake of particles by the tissues, we used coumarin-6 dye tagged MNPs. The results are discussed in terms of the amount of dye uptake by the tissues, as determined using a fluorescence plate reader. Muco-penetrating property was evaluated by tissue cross-section staining with Prussian blue.

The uptake of dye-tagged MNPs measured per gram of GI tissue with time at fixed concentration of MNPs was displayed in Fig. 7A. Freshly collected porcine GI tissue was chosen for this experiment, because it has very strong intact mucus barrier layer and all the studies were performed by maintaining mucus layer on the top side, so that the results could reflect the *in vivo* behavior [66,67]. The GI tissue took up approximately 50 μg of dye MNPs within 30 min. This was increased moderately to 65 μg over a period of 6 h. The MNPs+β-CD-F-127 formulation has shown a higher amount of uptake by GI tissue than other MNP+β-CD formulations in validated *in vitro* mucin binding studies. For further insight, the concentration of dye MNPs was varied from 10 to 30 μg/ml to examine the uptake of particles by GI tissue for 3 h (Fig. 7B). As the concentration of dye MNPs increased, the amount of uptake of dye MNPs was increased from 30 to 80 μg. This was further proven by the increased intensity of the blue color of Prussian blue stained images (Fig. 7B, inserts).

The same experiment was carried out in the ovarian, pancreas, and colon tissues of a pig (Fig. 7C). Similarly, the uptake of dye MNPs increased with increasing concentration of MNPs but the amount of uptake is relatively lower compared to GI tissue. This may be due to variation in the presence of mucin composition and the thickness of mucin on these tissues compared to GI tissue.

3.7. Transport of MNPs through mucin by Boyden chamber studies

The transport behavior of nanoparticles through mucin can be evaluated using multiple particle tracking [36,39], glass capillaries [51], confocal microscopy [21], Franz diffusion cell [68], etc. In the present study, we used Boyden's chamber to quantify the amount of MNPs transported. This technique was generally used to study the migration of cells through the micro porous membrane by placing cells in the upper compartment, and then allowing them to migrate through the pores of the membrane into the lower compartment. The lower compartment contained chemotactic agents. The number of cells migrated after an appropriate incubation time to the lower side of the membrane [69]. Mucin concentration (0.5 and 1 mg/ml) layers at a fixed coumarin-6 dye tagged MNPs are used in this assay and the results are discussed in terms of the amount of dye MNPs transported in the lower chamber (Fig. 8A and B). At both concentrations of mucin, MNPs are transported within 30 min and the amount transported increased slowly with time up to 24 h in the order of MNPs +β-CD-F-127 > MNPs+β-CD. The transport or diffusion of nanoparticles depends on the size and extent of their binding with the mucin fibers. It has been assumed that the stronger and higher the number of binding established between mucin and the nanosystems, the greatest the impairment to diffusion will be. It is an attempt to study the transport of particles through Boyden chamber experiments. In order to study the transport of particles mucin films can also be used. However, there are multiple parameters such as thickness, dimensional stability of films or membranes and the positioning of the membranes have to be standardized for this. We will consider these factor in our future course of studies.

An interesting transport behavior of different MNPs has been observed. Even though the interactions and binding of mucin on MNPs+β-CD is less compared to other MNPs particles, these have transported less, whereas MNPs+β-CD-F-127 particles have shown slightly higher binding and interactions with mucin, these particles are transported more in the mucin solution. This further confirms the decreased binding of mucin with time observed for MNPs+β-CD-F-127 particles. It has been widely demonstrated that poly (ethylene glycol) coating on nanoparticles will increase the transport of nanoparticles through the mucin [34,36,47,63,70,71]. It was also established that pretreatment of F-127 with cervicovaginal fluids increased the transport of nanoparticles through mucin [41]. Hence, because of the presence of F-127 on MNPs+β-CD-F-127, and also the poly(ethylene glycol) regions, these MNPs might have transported more compared to MNPs+β-CD [41]. Overall, the binding and transport of MNPs with mucin is highly complex, because the mucin itself is heterogeneous in nature and the individual nanoparticles are made with different components of core and surfaces. All these parameters might be playing their role in final observed behavior of the MNPs with mucin. Based on all the results, a schematic representation of the transport behavior of these MNPs in epithelial mucin layer was depicted hypothetically, and represented in Fig. 9.

4. Conclusions

It was hypothesized that PEGylated nano- and micro-particle exhibit superior mucoadhesion and facilitated mucosal transport for improved drug delivery. Considering this aspect, we have engineered a unique, magnetic nanoparticle formulation, comprised of PEG groups in

pluronic polymers but β-cyclodextrin which has shown improved therapeutic benefit of loaded therapeutic molecules. Toward developing this nanoparticle formulation for mucosal delivery we examined mucoadhesive and mucus transportation behavior. This study demonstrated the mucin binding and transporting behavior of magnetic nanoparticles developed with different surfaces by coating β-cyclodextrin, pluronic 127, and both together. Overall, MNPs+β-CD-F-127 formulation exhibited remarkable mucus binding characteristics over other examined nanoparticles. This was further evident from *ex-vivo* uptake studies of these MNPs by GI, ovarian, pancreas, and colon tissue. Prussian blue stained tissues are visually evident for the transportation of MNPs through mucus layer(s). A secondary measure of transportation assay by Boyden's chamber assay confirms that the MNPs+β-CD-F-127 formulation is better than other MNPs. These results suggest that these magnetic nanoparticles will be a good choice for mucosal targeting drug delivery and therapeutic applications.

Acknowledgments

This work was supported by Raman Postdoctoral Fellowship award (F.No. 5-1/2013 (IC)) granted to BVKN by University Grants Commission, Government of India, New Delhi. This work was partially supported by grants from the National Institutes of Health (K22 CA174841 to MMY, U01 CA162106A to SCC and MJ), and the College of Pharmacy 2015 Dean's Seed Grant of the University of Tennessee Health Science Center (to MMY, SCC, and MJ). Authors highly acknowledge Lisa L. Schaffer for editorial assistance.

References

[1]. Bansil R, Stanley HE, Lamont JT. Mucin biophysics. Annu. Rev. Physiol. 1995; 57:635–657. [PubMed: 7778881]

[2]. Chen EY, Daley D, Wang YC, Garnica M, Chen CS, Chin WC. Functionalized carboxyl nanoparticles enhance mucus dispersion and hydration. Scientific Reports. 2012; 2:211. [PubMed: 22355725]

[3]. Lai SK, Wang YY, Wirtz D, Hanes J. Micro- and macrorheology of mucus. Adv. Drug Deliver Rev. 2009; 61(2):86–100.

[4]. Verdugo P. Goblet cells secretion and mucogenesis. Annu. Rev. Physiol. 1990; 52:157–176. [PubMed: 2184755]

[5]. Larhed AW, Artursson P, Bjork E. The influence of intestinal mucus components on the diffusion of drugs. Pharm. Res. 1998; 15(1):66–71. [PubMed: 9487548]

[6]. Quraishi MS, Jones NS, Mason J. The rheology of nasal mucus: a review. Clin. Otolaryngol. Allied Sci. 1998; 23(5):403–413. [PubMed: 9800075]

[7]. Samet JM, Pepelko WE, Sonawane B, Hatch GE, Driscoll KE, Oberdorster G. Risk assessment of oxidant gases and particulate air pollutants: uncertainties and research needs. Environ. Health Perspect. 1994; 102(Suppl. 10):209–213.

[8]. Gu M, Yildiz H, Carrier R, Belfort G. Discovery of low mucus adhesion surfaces. Acta Biomater. 2013; 9(2):5201–5207. [PubMed: 23072828]

[9]. Boegh M, Nielsen HM. Mucus as a barrier to drug delivery – understanding and mimicking the barrier properties. Basic Clin. Pharmacol. Toxicol. 2015; 116(3):179–186. [PubMed: 25349046]

[10]. Cone RA. Barrier properties of mucus. Adv. Drug Deliv. Rev. 2009; 61(2):75–85. [PubMed: 19135107]

[11]. Donaldson SH, Bennett WD, Zeman KL, Knowles MR, Tarran R, Boucher RC. Mucus clearance and lung function in cystic fibrosis with hypertonic saline. New Engl. J. Med. 2006; 354(3):241–250. [PubMed: 16421365]

[12]. Knowles MR, Boucher RC. Mucus clearance as a primary innate defense mechanism for mammalian airways. J. Clin. Invest. 2002; 109(5):571–577. [PubMed: 11877463]

[13]. Pasquier MC, Vatier J. The gastrointestinal mucus: a complex protective barrier. 1: structure and physico-chemical properties. Gastroenterol. Clin. Biol. 1990; 14(4):352–358. [PubMed: 2190856]

[14]. Randell SH, Boucher RC. Effective mucus clearance is essential for respiratory health. Am. J. Resp. Cell Mol. 2006; 35(1):20–28.

[15]. Barnes PJ. Small airways in COPD. New Engl. J. Med. 2004; 350(26):2635–2637. [PubMed: 15215476]

[16]. Chaudhury NM, Shirlaw P, Pramanik R, Carpenter GH, Proctor GB. Changes in saliva rheological properties and mucin glycosylation in dry mouth. J. Dent. Res. 2015; 94(12):1660–1667. [PubMed: 26446936]

[17]. Chen EYT, Yang N, Quinton PM, Chin WC. A new role for bicarbonate in mucus formation. Am. J. Physiol. – Lung C. 2010; 299(4):L542–L549.

[18]. Yakubov GE, Papagiannopoulos A, Rat E, Easton RL, Waigh TA. Molecular structure and rheological properties of short-side-chain heavily glycosylated porcine stomach mucin. Biomacromolecules. 2007; 8(11):3467–3477. [PubMed: 17910495]

[19]. Fahy JV, Dickey BF. MEDICAL PROGRESS airway mucus function and dysfunction. New Engl. J. Med. 2010; 363(23):2233–2247. [PubMed: 21121836]

[20]. Hogg JC. Pathophysiology of airflow limitation in chronic obstructive pulmonary disease. Lancet. 2004; 364(9435):709–721. [PubMed: 15325838]

[21]. Mura S, Hillaireau H, Nicolas J, Kerdine-Romer S, Le Droumaguet B, Delomenie C, Nicolas V, Pallardy M, Tsapis N, Fattal E. Biodegradable nanoparticles meet the bronchial airway barrier: how surface properties affect their interaction with mucus and epithelial cells. Biomacromolecules. 2011; 12(11):4136–4143. [PubMed: 21981120]

[22]. Pruitt B, Jacobs M. Clearing away pulmonary secretions. Nursing. 2005; 35(7):36–41. quiz 41–2.

[23]. Andrianifahanana M, Chauhan SC, Choudhury A, Moniaux N, Brand RE, Sasson AA, Pour PM, Batra SK. MUC4-expressing pancreatic adenocarcinomas show elevated levels of both T1 and T2 cytokines: potential pathobiologic implications. Am. J. Gastroenterol. 2006; 101(10):2319–2329. [PubMed: 17032197]

[24]. Brown MA, Sakpal SV, Chamberlain RS. Mucobilia: current aspects in the management of a rare cause of malignant biliary obstruction. J. Hepato-Biliary-Pancreatic Sci. 2010; 17(3):205–210.

[25]. Chakraborty S, Bonthu N, Swanson BJ, Batra SK. Role of mucins in the skin during benign and malignant conditions. Cancer Lett. 2011; 301(2):127–141. [PubMed: 21146919]

[26]. Chauhan SC, Vannatta K, Ebeling MC, Vinayek N, Watanabe A, Pandey KK, Bell MC, Koch MD, Aburatani H, Lio Y, Jaggi M. Expression and functions of transmembrane mucin MUC13 in ovarian cancer. Cancer Res. 2009; 69(3):765–774. [PubMed: 19176398]

[27]. Choudhury A, Moniaux N, Ulrich AB, Schmied BM, Standop J, Pour PM, Gendler SJ, Hollingsworth MA, Aubert JP, Batra SK. MUC4 mucin expression in human pancreatic tumours is affected by organ environment: the possible role of TGFbeta2. Br. J. Cancer. 2004; 90(3):657–664. [PubMed: 14760381]

[28]. Kaur S, Kumar S, Momi N, Sasson AR, Batra SK. Mucins in pancreatic cancer and its microenvironment. Nature Rev. Gastroenterol. Hepatol. 2013; 10(10):607–620. [PubMed: 23856888]

[29]. Khan S, Ebeling MC, Chauhan N, Thompson PA, Gara RK, Ganju A, Yallapu MM, Behrman SW, Zhao H, Zafar N, Singh MM, Jaggi M, Chauhan SC. Ormeloxifene suppresses desmoplasia and enhances sensitivity of gemcitabine in pancreatic cancer. Cancer Res. 2015; 75(11):2292–2304. [PubMed: 25840985]

[30]. Kim YS, Ho SB. Intestinal goblet cells and mucins in health and disease: recent insights and progress. Curr. Gastroenterol. Rep. 2010; 12(5):319–330. [PubMed: 20703838]

[31]. Mccool DJ, Forstner JF, Forstner GG. Regulated and unregulated pathways for Muc2 mucin secretion in human colonic Ls180 adenocarcinoma cells are distinct. Biochem. J. 1995; 312:125–133. [PubMed: 7492301]

[32]. Remmers N, Anderson JM, Linde EM, DiMaio DJ, Lazenby AJ, Wandall HH, Mandel U, Clausen H, Yu F, Hollingsworth MA. Aberrant expression of mucin core proteins and o-linked

glycans associated with progression of pancreatic cancer. Clin. Cancer Res.: Official J. Am. Assoc. Cancer Res. 2013; 19(8):1981–1993.

[33]. Liu SY, Jones L, Gu FX. Development of mucoadhesive drug delivery system using phenylboronic acid functionalized poly(d, l-lactide)-b-dextran nanoparticles. Macromol. Biosci. 2012; 12(12):1622–1626. [PubMed: 23165800]

[34]. Shan W, Zhu X, Liu M, Li L, Zhong J, Sun W, Zhang Z, Huang Y. Overcoming the diffusion barrier of mucus and absorption barrier of epithelium by self-assembled nanoparticles for oral delivery of insulin. ACS Nano. 2015; 9(3):2345–2356. [PubMed: 25658958]

[35]. Tang BC, Dawson M, Lai SK, Wang YY, Suk JS, Yang M, Zeitlin P, Boyle MP, Fu J, Hanes J. Biodegradable polymer nanoparticles that rapidly penetrate the human mucus barrier. P Natl. Acad. Sci. USA. 2009; 106(46):19268–19273.

[36]. Xu Q, Ensign LM, Boylan NJ, Schon A, Gong X, Yang JC, Lamb NW, Cai S, Yu T, Freire E, Hanes J. Impact of surface polyethylene glycol (PEG) density on biodegradable nanoparticle transport in mucus ex vivo and distribution in vivo. ACS Nano. 2015; 9(9):9217–9227. [PubMed: 26301576]

[37]. Thasneem YM, Rekha MR, Sajeesh S, Sharma CP. Biomimetic mucin modified PLGA nanoparticles for enhanced blood compatibility. J. Colloid Interface Sci. 2013; 409:237–244. [PubMed: 23978287]

[38]. Wang YY, Lai SK, So C, Schneider C, Cone R, Hanes J. Mucoadhesive nanoparticles may disrupt the protective human mucus barrier by altering its microstructure. PLoS ONE. 2011; 6(6)

[39]. Yang M, Yu T, Wang YY, Lai SK, Zeng Q, Miao B, Tang BC, Simons BW, Ensign LM, Liu G, Chan KW, Juang CY, Mert O, Wood J, Fu J, McMahon MT, Wu TC, Hung CF, Hanes J. Vaginal delivery of paclitaxel via nanoparticles with non-mucoadhesive surfaces suppresses cervical tumor growth. Adv. Healthcare Mater. 2014; 3(7):1044–1052.

[40]. Yoncheva K, Lizarraga E, Irache JM. Pegylated nanoparticles based on poly (methyl vinyl ether-co-maleic anhydride): preparation and evaluation of their bioadhesive properties. Eur. J. Pharm. Sci.: Official J. Eur. Federat. Pharm. Sci. 2005; 24(5):411–419.

[41]. Ensign LM, Lai SK, Wang YY, Yang M, Mert O, Hanes J, Cone R. Pretreatment of human cervicovaginal mucus with pluronic F127 enhances nanoparticle penetration without compromising mucus barrier properties to herpes simplex virus. Biomacromolecules. 2014; 15(12):4403–4409. [PubMed: 25347518]

[42]. Yallapu MM, Chauhan N, Othman SF, Khalilzad-Sharghi V, Ebeling MC, Khan S, Jaggi M, Chauhan SC. Implications of protein corona on physico-chemical and biological properties of magnetic nanoparticles. Biomaterials. 2015; 46:1–12. [PubMed: 25678111]

[43]. das Neves J, Amiji M, Sarmento B. Mucoadhesive nanosystems for vaginal microbicide development: friend or foe? Wiley interdisciplinary reviews. Nanomed. Nanobiotechnol. 2011; 3(4):389–399.

[44]. Lacerda SH, Park JJ, Meuse C, Pristinski D, Becker ML, Karim A, Douglas JF. Interaction of gold nanoparticles with common human blood proteins. ACS Nano. 2010; 4(1):365–379. [PubMed: 20020753]

[45]. Lai SK, O'Hanlon DE, Harrold S, Man ST, Wang YY, Cone R, Hanes J. Rapid transport of large polymeric nanoparticles in fresh undiluted human mucus. P Natl. Acad. Sci. USA. 2007; 104(5): 1482–1487.

[46]. Ponchel G, Montisci MJ, Dembri A, Durrer C, Duchene D. Mucoadhesion of colloidal particulate systems in the gastro-intestinal tract. Eur. J. Pharm. Biopharm. 1997; 44(1):25–31.

[47]. Wang YY, Lai SK, Suk JS, Pace A, Cone R, Hanes J. Addressing the PEG Mucoadhesivity Paradox to Engineer Nanoparticles that “Slip” through the Human Mucus Barrier. Angew. Chem. Int. Edit. 2008; 47(50):9726–9729.

[48]. Ensign LM, Cone R, Hanes J. Oral drug delivery with polymeric nanoparticles: the gastrointestinal mucus barriers. Adv. Drug Deliver Rev. 2012; 64(6):557–570.

[49]. Peppas NA, Huang YB. Nanoscale technology of mucoadhesive interactions. Adv. Drug Deliver Rev. 2004; 56(11):1675–1687.

[50]. Serra L, Domenech J, Peppas NA. Engineering design and molecular dynamics of mucoadhesive drug delivery systems as targeting agents. Eur. J. Pharm. Biopharm. 2009; 71(3):519–528. [PubMed: 18976706]

[51]. Cu Y, Saltzman WM. Controlled surface modification with poly(ethylene) glycol enhances diffusion of PLGA nanoparticles in human cervical mucus. Mol. Pharm. 2009; 6(1):173–181. [PubMed: 19053536]

[52]. Mahmoudi M, Lynch I, Ejtehadi MR, Monopoli MP, Bombelli FB, Laurent S. Protein-nanoparticle interactions: opportunities and challenges. Chem. Rev. 2011; 111(9):5610–5637. [PubMed: 21688848]

[53]. Cui FY, Qian F, Yin CH. Preparation and characterization of mucoadhesive polymer-coated nanoparticles. Int. J. Pharm. 2006; 316(1–2):154–161. [PubMed: 16567070]

[54]. Ludwig A. The use of mucoadhesive polymers in ocular drug delivery. Adv. Drug Deliver Rev. 2005; 57(11):1595–1639.

[55]. Ibrahim N, Ibrahim H, Kim S, Nallet JP, Nepveu F. Interactions between antimalarial indolone-N-oxide derivatives and human serum albumin. Biomacromolecules. 2010; 11(12):3341–3351. [PubMed: 21080702]

[56]. Brewer SH, Glomm WR, Johnson MC, Knag MK, Franzen S. Probing BSA binding to citrate-coated gold nanoparticles and surfaces. Langmuir: ACS J. Surf. Colloids. 2005; 21(20):9303–9307.

[57]. Clayton AHA, Sawyer WH. Site-specific tryptophan fluorescence spectroscopy as a probe of membrane peptide structure and dynamics. Eur. Biophys. J. Biophys. 2002; 31(1):9–13.

[58]. Roach P, Farrar D, Perry CC. Interpretation of protein adsorption: surface-induced conformational changes. J. Am. Chem. Soc. 2005; 127(22):8168–8173. [PubMed: 15926845]

[59]. Jovanovic-Talisman T, Vukojevic V. Super-resolution fluorescence imaging and correlation spectroscopy: principles and examples of application. J. Serb. Chem. Soc. 2013; 78(11):1671–1688.

[60]. Mandeville JS, Froehlich E, Tajmir-Riahi HA. Study of curcumin and genistein interactions with human serum albumin. J. Pharmaceut. Biomed. 2009; 49(2):468–474.

[61]. N'soukpoe-Kossi CN, Sedaghat-Herati R, Ragi C, Hotchandani S, Tajmir-Riahi HA. Retinol and retinoic acid bind human serum albumin: Stability and structural features. Int. J. Biol. Macromol. 2007; 40(5):484–490. [PubMed: 17184834]

[62]. Almeida BG, Bacchi CE, Carvalho JP, Ferreira CR, Carvalho FM. The role of intratumoral lymphovascular density in distinguishing primary from secondary mucinous ovarian tumors. Clinics. 2014; 69(10):660–665. [PubMed: 25518016]

[63]. Lai SK, Wang YY, Hanes J. Mucus-penetrating nanoparticles for drug and gene delivery to mucosal tissues. Adv. Drug Deliver Rev. 2009; 61(2):158–171.

[64]. Mandal AK, Bhattacharyya A, Bhattacharyya S, Bhattacharyya T, Roy S. A cognate tRNA specific conformational change in glutaminyl-tRNA synthetase and its implication for specificity. Protein Sci.: Publ. Protein Soc. 1998; 7(4):1046–1051.

[65]. McGill SL, Smyth HD. Disruption of the mucus barrier by topically applied exogenous particles. Mol. Pharm. 2010; 7(6):2280–2288. [PubMed: 20919744]

[66]. Leung KC, Sham KW, Chak CP, Lai JM, Lee SF, Wang YX, Cheng CH. Evaluation of biocompatible alginate- and deferoxamine-coated ternary composites for magnetic resonance imaging and gene delivery into glioblastoma cells. Quant. Imag. Med. Surg. 2015; 5(3):382–391.

[67]. Yallapu MM, Ebeling MC, Khan S, Sundram V, Chauhan N, Gupta BK, Puumala SE, Jaggi M, Chauhan SC. Novel curcumin-loaded magnetic nanoparticles for pancreatic cancer treatment. Mol. Cancer Ther. 2013; 12(8):1471–1480. [PubMed: 23704793]

[68]. Zhang J, Lv Y, Wang B, Zhao S, Tan M, Lv G, Ma X. Influence of microemulsion-mucin interaction on the fate of microemulsions diffusing through pig gastric mucin solutions. Mol. Pharm. 2015; 12(3):695–705. [PubMed: 25608210]

[69]. Chen HC. Boyden chamber assay. Methods Mol. Biol. 2005; 294:15–22. [PubMed: 15576901]

[70]. Ehrenberg MS, Friedman AE, Finkelstein JN, Oberdorster G, McGrath JL. The influence of protein adsorption on nanoparticle association with cultured endothelial cells. Biomaterials. 2009; 30(4):603–610. [PubMed: 19012960]

[71]. Yang M, Lai SK, Yu T, Wang YY, Happe C, Zhong WX, Zhang M, Anonuevo A, Fridley C, Hung A, Fu J, Hanes J. Nanoparticle penetration of human cervicovaginal mucus: the effect of polyvinyl alcohol. J. Control Release. 2014; 192:202–208. [PubMed: 25090196]

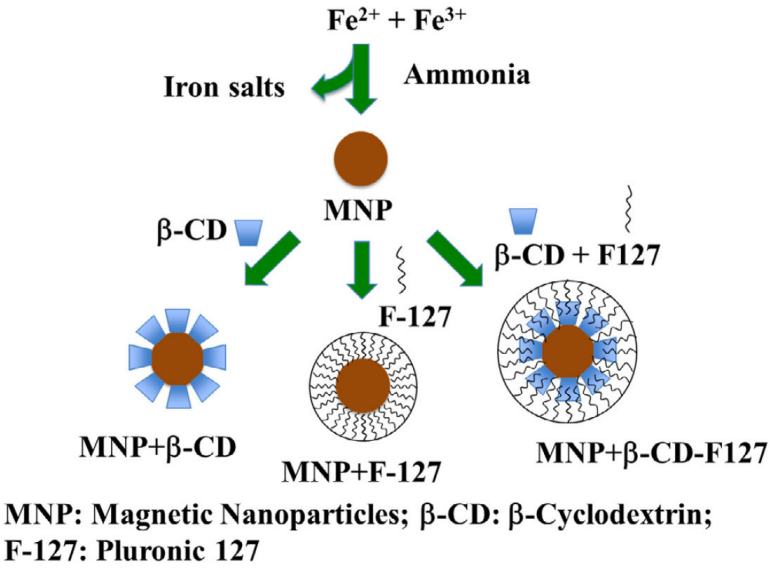

Fig. 1.

Schematic representation of the synthesis of magnetic nanoparticles (MNPs). Four different formulations of MNP were prepared, i.e., MNP core (no coating) or by coating the MNP surface either with β-cyclodextrin or with pluronic 127 and both together.

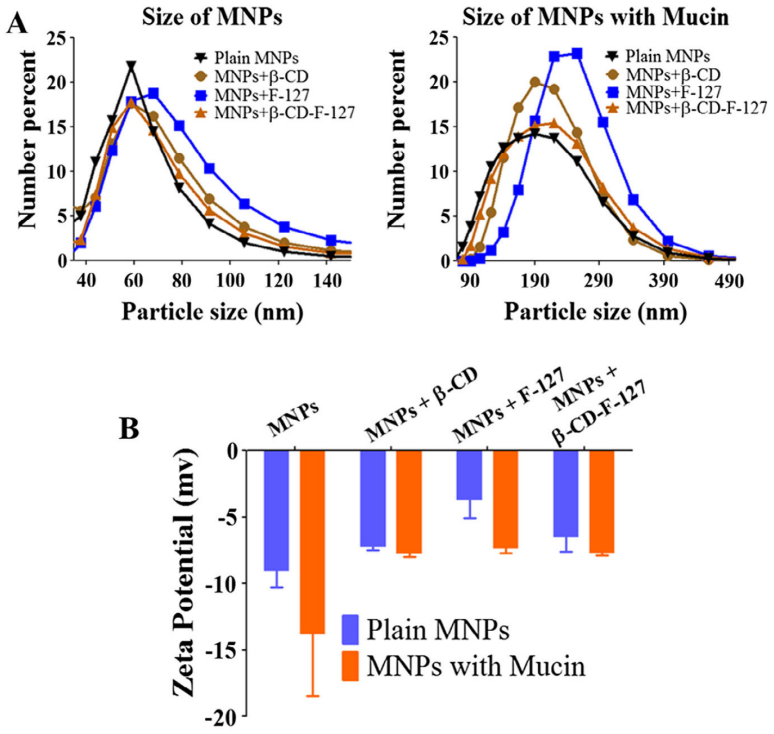

Fig. 2.

Particle size and zeta potential of MNPs and mucin bound MNPs. (A) Particle size of MNPs and mucin bound MNPs measured for 3 min using dynamic light scattering technique. (B) Zeta potential of different MNPs and mucin bound MNPs measured in 9 min. Data presented as an average of three independent measurements and error bars drawn are from standard error of the mean).

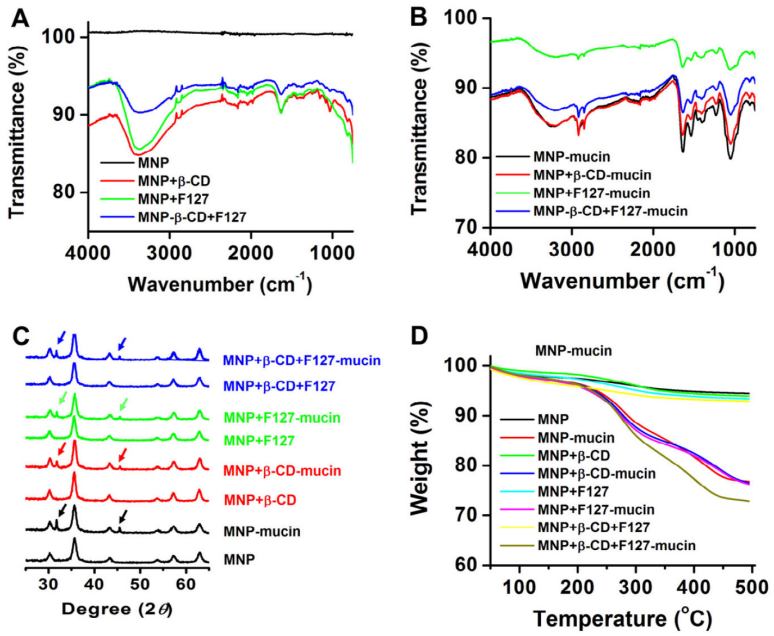

Fig. 3.

Spectral and thermal characterization of (A–B) FTIR spectra, (C) X-ray diffractograms, and (D) Thermograms of plain MNP, MNPs+β-CD, MNPs+F-127, MNPs+β-CD-F-127 and 500 μg mucin bound on the surface of nanoparticles. Note: Mucin presence was confirmed by all three analytical techniques.

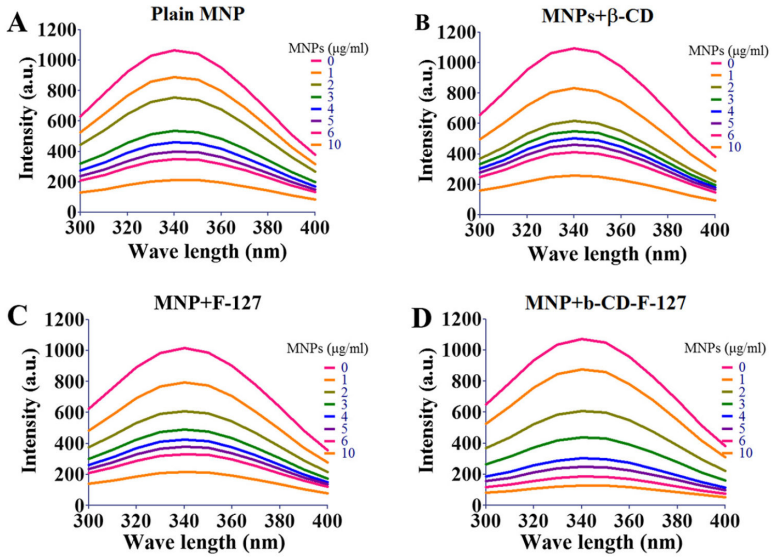

Fig. 4.

Results of steady state florescence quenching of 1 mg/ml mucin with (A) plain MNPs, (B) MNPs+β-CD, (C) MNPs+F-127 and (D) MNPs+β-CD-F-127 with increasing the concentration of MNPs from 10 × (0 to 10 μg/ml). A representative spectra of formulation was presented from three independent spectral analysis.

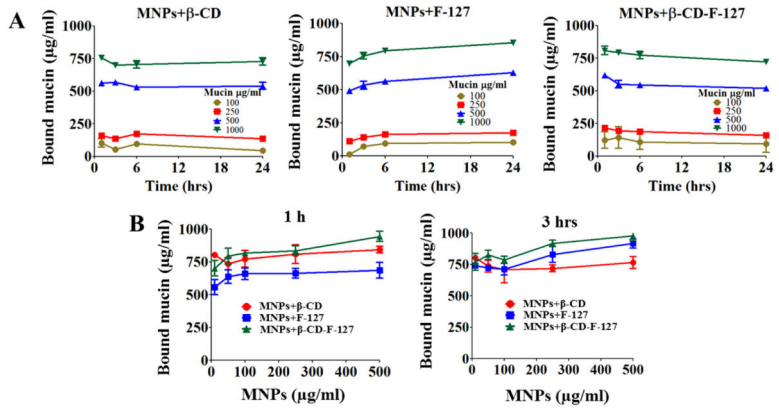

Fig. 5.

Amount of mucin binding onto the different MNPs. (A) Concentration of bound mucin expressed in μg/ml on to the MNPs+β-CD and MNPs+β-CD-F-127 particles, while varying the concentration of mucin from 100 to 1000 μg/ml at 1, 3, 6 and 24 h time points, at a fixed MNP concentration of 250 μg/ml. (B) Concentration of bound mucin expressed in μg/ml on to the MNPs+β-CD and MNPs+β-CD-F-127 particles, while varying the concentration of MNPs from 10 to 500 μg/ml at 1 and 3 h time points, at fixed mucin concentration of 1000 μg/ml. Data presented is average of three independent measurements and error bars drawn are from standard error of the mean.

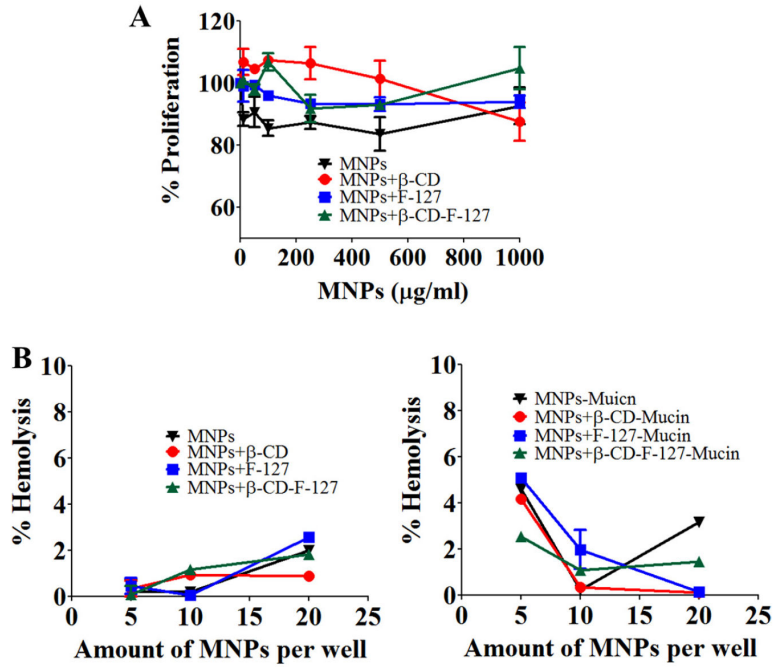

Fig. 6.

Toxicity studies of MNPs toward SiHa and red blood cells. (A) SiHa cell proliferation with varied concentration of MNPs after 48 h treatment measured by MTS assay. Data presented is average of five treatment wells and error bars drawn are from standard error of the mean). (B) Percentage hemolysis measured after treating the red blood cells with plain MNPs and mucin bound MNPs after 1 h of incubation of RBCs with particles. Data presented is average of five measurements and error bars drawn are from standard error of the mean.

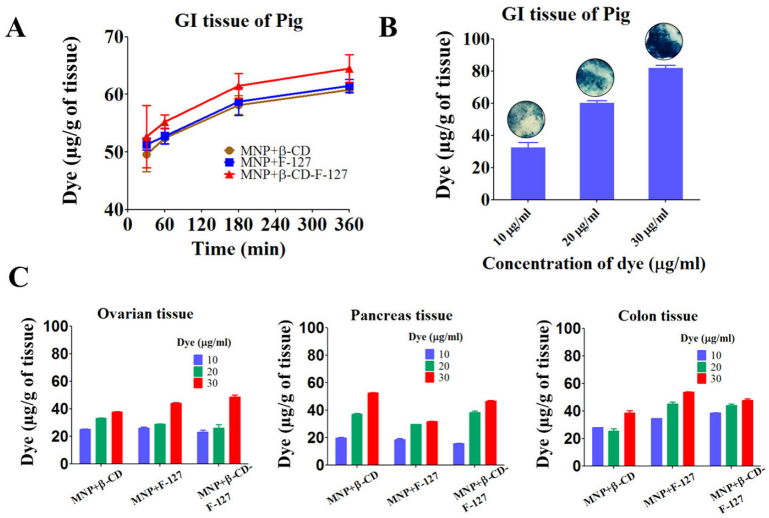

Fig. 7.

Ex vivo binding and uptake of coumarin-6 dye tagged MNPs with different pig organs. (A) Amount of dye uptake by the GI tissue of pig from MNPs+β-CD and MNPs+β-CD-F-127 dye tagged with time at fixed concentration of 20 µg/ml of dye. (B) Amount of dye uptake by the GI tissue from MNPs+β-CD-F-127 at 3 h with varied concentration of MNPs. The corresponding Prussian blue images of the tissue are inserted at the top of the each histogram. (C) Amount of dye uptake by the ovarian, pancreas, and colon tissues for MNPs +β-CD and MNPs+β-CD-F-127 with varied concentration of MNPs at 3 h. Data presented is average of three independent measurements and error bars drawn are from standard error of the mean. (For interpretation of the references to colour in this figure legend, the reader is referred to the web version of this article.)

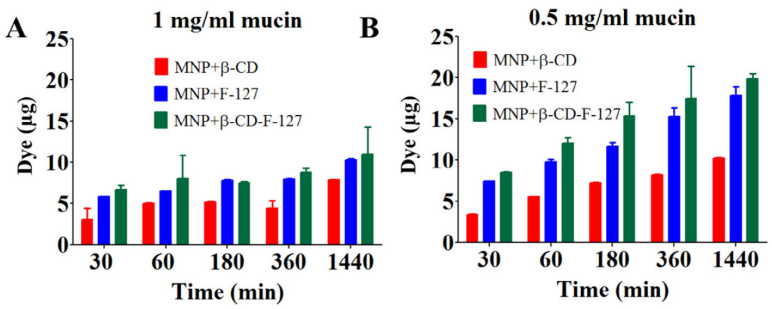

Fig. 8.

Transport phenomenon of MNPs in mucin solutions using Boyden's chamber method (A) Amount of dye transported from MNPs+β-CD and MNPs+β-CD-F-127 particles with time at 500 μg/ml MNPs in 1 mg/ml mucin solutions. (B) Amount of dye transported from MNPs +β-CD and MNPs+β-CD-F-127 particles with time at 500 μg/ml MNPs in 0.5 mg/ml mucin solutions. Data presented is average of three independent measurements and error bars drawn are from standard error of the mean.

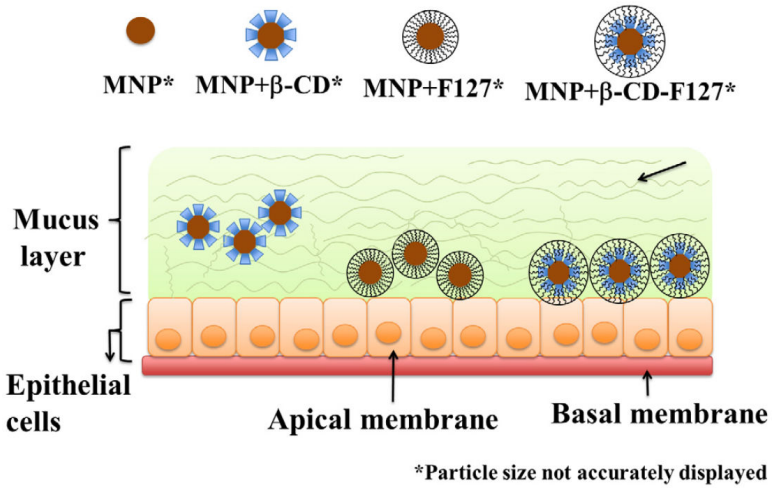

Fig. 9.

Schematic representation of binding and transport behavior of MNPs+β-CD, MNPs+F-127 and MNPs+β-CD-F-127 particles in the mucin layer of epithelia surface based on the observed results.

Table 1

Number of binding sites and binding constants of various MNPs calculated from steady state florescence quenching measurements data.

Formulation	Mucin binding[a]		Mucin binding[b]	
	Number of binding sites (n)	Binding constant (k)	Number of binding sites (n)	Binding constant (k)
MNPs+β-CD	1.295	0.017	1.356	0.012
MNPs+F-127	1.954	0.101	1.955	0.091
MNPs+β-CD-F-127	2.006	0.100	2.987	0.205

[a]Mucin concentration 0.5 mg/mL.

[b]Mucin concentration 1 mg/mL.